J Electroceram (2010) 24:161–169
DOI 10.1007/s10832-008-9551-x

Chemical solution deposition of copper thin films and integration into a multilayer capacitor structure

Song Won Ko · Tanawadee Dechakupt · Clive A. Randall · Susan Trolier-McKinstry · Michael Randall · Azizuddin Tajuddin

Received: 17 January 2008 / Accepted: 15 September 2008 / Published online: 9 October 2008

Abstract Metallization layers with thicknesses well below a micron are needed for future generation multilayer ceramic devices such as capacitors and integrated passive components. In many cases, the limiting thickness for the electrode is governed by dewetting of the metals from the oxide surface. Therefore, thin, stable metallization layers with low electrical resistivities that can survive high processing temperatures are of interest for these applications. For this purpose, Cu films prepared from 2-methoxyethanol-based solutions were developed using adhesion promoters such as Ti, Zn, and Zr. The solutions were spun onto $BaTiO_3/SiO_2/Si$ or SiO_2/Si substrates, pyrolyzed, and annealed in a reducing ambient. The microstructure of films prepared in this way was found to be uniform and continuous at thicknesses as low as 80 nm. Cu films modified with 15 mol% Zr had electrical resistivities of about 16–17 μΩ-cm after 500°C annealing and 5–6 μΩ-cm after annealing at 900°C in a reducing ambient.

Keywords Cu film · Multilayer capacitors · Electrical resistivity

S. W. Ko (✉) · T. Dechakupt · C. A. Randall · S. Trolier-McKinstry
Materials Science and Engineering Department, Materials Research Institute, The Pennsylvania State University, University Park, PA 16802, USA
e-mail: STMcKinstry@psu.edu

M. Randall · A. Tajuddin
KEMET Electronics Corporation, 2835 KEMET way, Simpsonville, SC 29681, USA

1 Introduction

The drive toward high volumetric efficiency in capacitors is enabled by continuous reductions in the thicknesses of both the dielectric and metallization layers [1–4]. The state of the art in powder-based production methods for $BaTiO_3$/Ni capacitors produces dielectric thicknesses of ~0.6 to 0.8 μm. There is continued interest in further reducing layer thicknesses to increase the capacitor volumetric efficiency [5]. At present, the progress in reducing the dielectric thickness has proceeded faster than attempts to reduce the thickness of Ni-based electrodes. The net result is that it is becoming increasingly more difficult to increase capacitance volumetric efficiency in MLCs.

One approach to continuing reduction of layer thicknesses is use of thin films. There are several reports of high permittivity $BaTiO_3$-based dielectric thin films on metal foils by chemical solution deposition. Clem and co-workers [6] reported that oriented $(Ba,Sr)TiO_3$ films on Ni foils had a dielectric constant over 1,000 and low dielectric loss up to 500 kV/cm. Permittivities of 1,000–2,000 were also reported by Nagata et al. and Dechakupt et al. for $BaTiO_3$ films on Ni foils [7, 8]. Ihlefeld et al. [9–11] described 600–650 nm thick $BaTiO_3$ films on Cu foils with dielectric constants as high as 2,500–3,000. Therefore, thin film technology combined with base metal electrodes seems to be a promising approach for down-scaling thicknesses in embedded capacitors, multilayer ceramic capacitors (MLC) and integrated passive components.

Low layer count thin film MLCs have been reported by a variety of researchers. Sakabe et al. [12] demonstrated a thin film MLC on an MgO substrate by alternative depositions of a $(Ba,Sr)TiO_3$ dielectric layer and Pt electrode using metalorganic chemical vapor deposition (MOCVD) and sputtering, respectively. The Pt deposition

was done through a shadow mask to define the capacitor features. The same group has subsequently reported thin film single and multilayer capacitors using $BaTiO_3$ thin films on thin Si substrates. Again, the electrodes are deposited by vacuum-based techniques [13]. Watt et al. [14] constructed a multilayer capacitor structure using a Pt/BST/Pt stack with up to four dielectric layers. In this case, the patterning was done from the top down on blanket films via photolithography and etching. Brennecka et al. have reported on the fabrication of Pt/PZT multilayer capacitors; again the work used chemical solution deposited dielectrics and vacuum-deposited electrodes with lithographic patterning [15, 16]. The costs associated with the vacuum deposition of the films, as well as the patterning steps may preclude use of this technology for some applications.

Adoption of thin films in MLC and integrated passive components would be facilitated by an economical means of patterning all of the layers. Micro-contact printing (μCP) of chemical solutions of the dielectric and electrode layers is one means of patterning thin film-based MLC without requiring photolithography [7]. It was previously reported that $LaNiO_3$ / $BaTiO_3$/ $LaNiO_3$ capacitor stacks can be prepared by the μCP process. Unfortunately, the poor stability of $LaNiO_3$ at ≥900°C suggests the need for an alternative metallization layer. Moreover, the electrical resistivity of 130 nm thick $LaNiO_3$ films prepared using a printable solution was around 600 μΩ-cm; this comparatively high resistivity is consistent with previous results [17]. Thus, there is a need for temperature-stable, higher conductivity metallization. This work focuses on the development of printable Cu solutions for this application.

Copper is now widely used for ultralarge-scale integrated circuits because of its low electrical resistivity and good electromigration resistance. One of the disadvantages of copper for application in thin film passive components is that copper is readily oxidized at low temperatures; formation of the oxide degrades the electrical conductivity [18, 19]. In addition, metallic copper generally has poor adhesion to oxide surfaces due to a high contact angle [20–23]. Therefore, for copper thin film electrodes to be relevant in these applications, it is imperative that good continuity of Cu be retained on an oxide surface, while preventing the formation of Cu_2O or CuO.

To address these problems, Cu has been alloyed with elements such as Al, Ti, Cr, etc., which have a strong affinity with oxygen [24, 25], to improve adhesion by decreasing the contact angle between the metal and oxide surfaces. In addition, these elements have a stronger affinity to oxygen than does copper, and so may be useful to minimize copper oxidation. Alternatively, Cr or Ti layers can be deposited on SiO_2 [26, 27] or graphite [28] before copper deposition to improve the wettability of copper films. In a similar fashion, Kwon et al. [29] and Wang et al. [30] investigated Ru and Pd thin films as adhesion layers, respectively.

Most of the reported methods for growing copper films are vacuum based, including chemical vapor deposition, sputtering, and ion beam deposition [31–35]. These approaches are incompatible with microcontact printing. Therefore, this paper describes a chemical solution deposition (CSD) process for copper films. This work should be useful in single or multilayer electronic devices as the films are thin, continuous and conductive.

2 Experimental procedure

Copper nitrate hydrate [Aldrich, 99.999%] was used as a precursor and 2-methoxyethanol [Aldrich, 99.9%] was used as a solvent. To prepare solutions, the copper nitrate hydrate was dissolved in 2-methoxyethanol, and the liquid stirred for ~1 h at 105°C under flowing Ar. The molarity of the final solution was ~0.3 M.

Copper films were prepared on SiO_2/Si substrates (Nova Electronic Materials, Carrollton, Texas) by spin-coating at 3,000 rpm for 30 s. After each deposition, the film was dried at 280°C for 3 min on a hotplate in air. Following the deposition of four layers (~40 nm), the film was annealed at 750°C for 1 min in a rapid thermal annealer (RTA) in an atmosphere with 5% hydrogen forming gas. Initial work showed that the resulting films were free of copper oxides in the X-ray diffraction pattern. However, the Cu forms discontinuous islands. In the same way, copper films annealed at lower temperatures (~500°C) with low heating rates (5°C/min), dewet from oxide surfaces as shown in Fig. 1(a).

Therefore, the copper solutions were modified with a variety of adhesion promoters/film stabilizers. In general, elements with a strong affinity for oxygen, like Ti and Cr, are used as adhesion promoters for metals on oxide surfaces [36, 37]. In this work, the copper solutions were modified using Ti isopropoxide (Aldrich, 99.999%), Zr propoxide (Aldrich, 70 wt% solution in 1-propanol), or zinc acetate dehydrate (Aldrich, 99.999%) as adhesion promoters. To do this, the copper nitrate hydrate was dissolved in 2-methoxyethanol, and the solution was stirred for ~1 h at 105°C in an Ar atmosphere. After that, an adhesion promoter (Ti isopropoxide, Zr propoxide, or zinc acetate dehydrate) was added to the copper solution and then stirred for at least 30 min at 105°C in an Ar atmosphere. The resulting solutions were typically ~0.3 M.

To assess the continuity of modified Cu films on oxide surfaces, thin films were prepared on either SiO_2/Si substrates or $BaTiO_3$/SiO_2/Si substrates. After each deposition, the films were typically pyrolyzed at 250–350°C, and

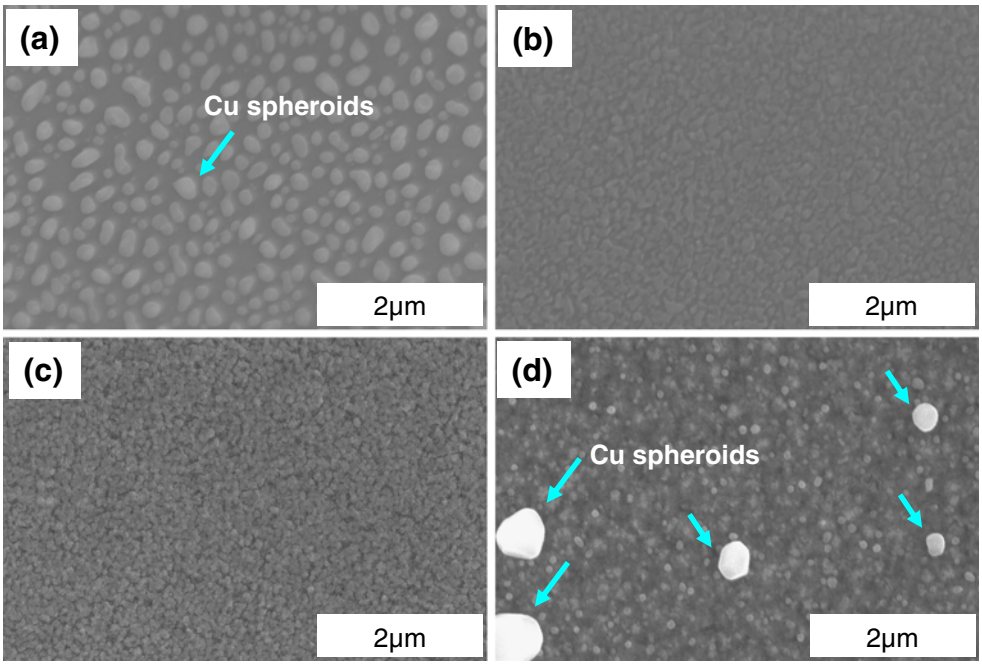

Fig. 1 SEM images of (**a**) a Cu film and (**b**) a 5 m/o Ti–Cu film on SiO_2/Si substrates, (**c**) a 5 m/o Ti–Cu film and (**d**) a 10 m/o Ti–Cu film on $BaTiO_3$/SiO_2/Si substrates annealed at 500°C in a reducing ambient

multiple cycles were used to build up larger layer thicknesses. The films were crystallized in a tube furnace between 500 and 900°C in a reducing ambient. Typical oxygen partial pressures were ~10^{-30} atm at 500°C and ~10^{-17} atm at 900°C. These were achieved by flowing gas mixtures of hydrogen and nitrogen.

The resulting films were characterized for their structural and microstructural properties. The film thicknesses were measured by profilometry (Alpha-step 500 surface profiler, Tencor). The crystallinity was characterized with a Scintag DMC-105 x-ray diffractometer using Cu Kα radiation. The 2θ scan range was 20° to 60° with a step size of 0.02° and a count time of 0.5 s per step. The surface morphology of the films was examined with a Hitachi S-3500N Scanning Electron Microscope. Fourier transform infrared (IFS 66/s, Bruker) and attenuated total reflectance (Veemax II, Pike technologies) techniques were used to check for organic groups in the copper films. The electrical conductivity was measured using a four-point probe (Resistivity test unit, Jandel Engineering Ltd.). Cross-sectional TEM samples of $BaTiO_3$/Cu/$BaTiO_3$ capacitor on sapphire substrate were prepared using an FEI Quanta 200 3D dual beam FIB.

3 Results and discussion

3.1 Ti-doped Cu films

To assess their continuity, Ti-doped copper films were prepared on SiO_2/Si and $BaTiO_3$/SiO_2/Si substrates. Figure 1 shows a comparison of the microstructures of pure Cu films and Ti-doped Cu film on SiO_2/Si and $BaTiO_3$/SiO_2/Si substrates. All samples were annealed at 500°C in a reducing ambient (hydrogen 20 sccm, wet nitrogen 50 sccm, and dry nitrogen 430 sccm). The presence of Cu, without any of its oxides, was confirmed within the sensitivity limits of X-ray diffraction. As can be seen in Fig. 1(a), under these conditions the pure Cu film is discontinuous, leading to electrically isolated copper islands. In contrast, even for a 40 nm thick film, the dewetting of Cu can be avoided using 5 m/o Ti modification of the solution as shown in Fig. 1(b). On the $BaTiO_3$-coated substrate, the 10 m/o Ti–Cu film is continuous, although some Cu globules are clearly visible in Fig. 1(d). Subsequent experiments showed that the amount of Cu protrusions from the film was very difficult to control, and varied considerably from sample to sample. It is important to note that the microstructural heterogeneity develops during the heat treatment step. That is, in all cases, the CSD films showed good continuity and flatness on both substrates after spin-coating and pyrolysis. It was only on crystallization at 500°C that the microstructural heterogeneity developed.

The Ti-doped Cu films in Fig. 1(c) and (d) were 250 to 280 nm thick. The electrical resistivities were 50–84 μΩ-cm for the 5 m/o Ti–Cu film and 150–250 μΩ-cm for the 10 m/o Ti–Cu film. Both of these are considerably below those of $LaNiO_3$ films, suggesting that modified CSD Cu is of interest for high conductivity films.

While dewetting of Cu from these oxide surfaces could be avoided using Ti modified solutions for films annealed at 500°C, the microstructure was not stable at higher temperatures. Figure 2 shows the microstructures of Ti-doped Cu films on different substrates annealed at 800°C.

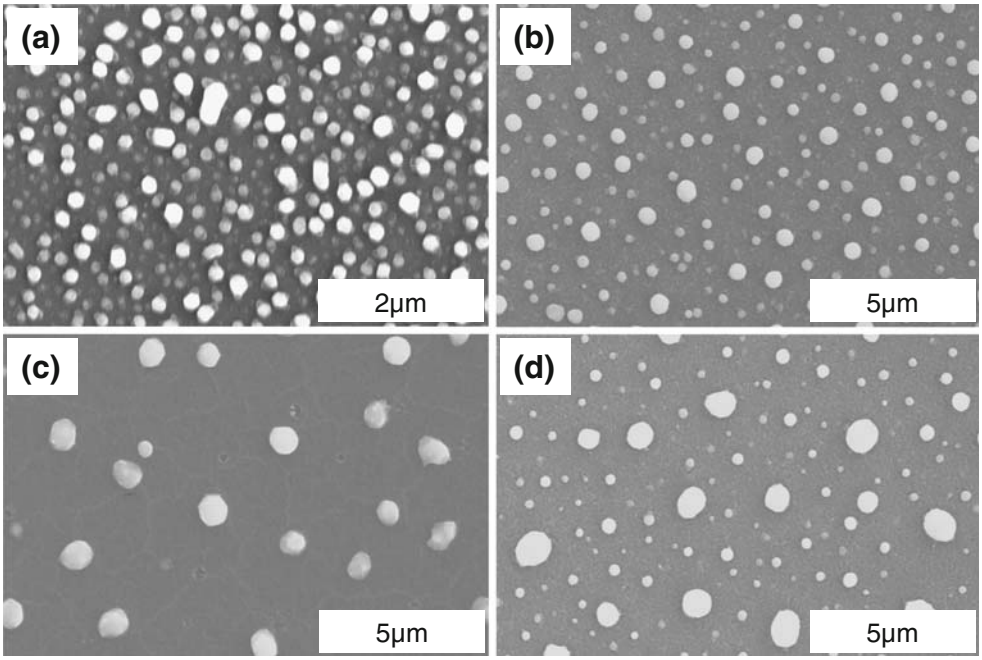

Fig. 2 SEM images of 5 m/o Ti–Cu films on (**a**) SiO_2/Si, (**b**) $BaTiO_3/SiO_2$/Si, (**c**) TiO_2/SiO_2/Si, and (**d**) 10 m/o Ti–Cu film on $BaTiO_3/SiO_2$/Si substrate annealed at 800°C in $Po_2 \sim 10^{-17}$ atm

Dewetting of Cu develops irrespective of the Ti content. In this figure, the spheroidal features are Cu-rich islands. Unfortunately, such high temperatures are generally required to produce $BaTiO_3$ films with permittivities >1,000. Thus, alternative adhesion promoters were examined.

3.2 Zn-doped Cu films

Zn-doped copper films were prepared on SiO_2/Si substrates. A gradual transition from lacy to fully coverage Cu films was observed as the Zn content was raised from 5 to 30 m/o films. These samples were annealed at 500°C in a reducing ambient (hydrogen 20 sccm, wet nitrogen 50 sccm, and dry nitrogen 430 sccm). The microstructure of a 60 nm thick 5 m/o Zn–Cu film is porous but continuous, and its electrical resistivity was about 7 μΩ-cm. The resistivity of Zn-doped Cu films increases slowly with the Zn content (i.e. the resistivity of a 60 nm thick 30 m/o Zn–Cu film was about 10–11 μΩ-cm). Again, there are no copper oxide peaks in the XRD pattern. Unfortunately, it was observed that the continuity of Zn-doped Cu films also degraded unacceptably during high temperature annealing.

3.3 Zr-doped Cu films

Zr-doped copper films were prepared on SiO_2/Si substrates. Dewetting of Cu at 500°C can be avoided using Zr modified solutions as well as Ti or Zn modified solutions. However, directly heating the film to high temperatures again resulted in dewetting. To avoid the breakup of the Cu film at elevated temperatures, an attempt was made to stabilize the microstructure first using a lower temperature anneal. In the modified annealing procedure, the film was heated to 500°C and then cooled to room temperature. It was then reheated to 900°C and finally cooled down. All steps proceed in a reducing ambient to prevent oxide formation. The reducing ambients were an oxygen partial pressure of $\sim 10^{-30}$ atm for the 500°C annealing temperature and an oxygen partial pressure of $\sim 10^{-17}$ atm for the 900°C step.

Figure 3(a)–(f) show the microstructures of Zr-doped Cu films with different compositions using the modified annealing step. It is clear that dewetting of Cu from the oxide-coated substrates can be avoided. Dark areas in the micrographs correspond to exposed substrate, and so indicate discontinuity of the Cu film. The maximum processing temperature of uniform and continuous Cu films previously reported was less than 400°C [13–15], so this approach provides a considerable improvement. It is also clear from Fig. 3 that as the Zr content increases, the continuity of the Zr modified Cu improves.

Figure 4 shows the resistivity of 80 nm thick Cu films with different Zr contents. As the annealing temperature increases, the resistivities of all films decrease. The resistivity of the 5 m/o Zr–Cu film annealed at 900°C could not be measured because the Cu was too discontinuous, as shown in Fig. 3(a). It was found that the 15 m/o Zr–Cu film had the lowest resistivity: about 16–17 μΩ-cm for annealing at 500°C and 5–6 μΩ-cm after the 900°C heat treatment. The bulk resistivity of Cu is 1.67 μΩ-cm (http://en.wikipedia.org/wiki/Copper). The resistivities of Cu films deposited by sputtering or ion beam deposition are typically 2–3 μΩ-cm for film thicknesses of 80–120 nm [16, 17, 38]. The low electrical resistivities of the CSD Cu films

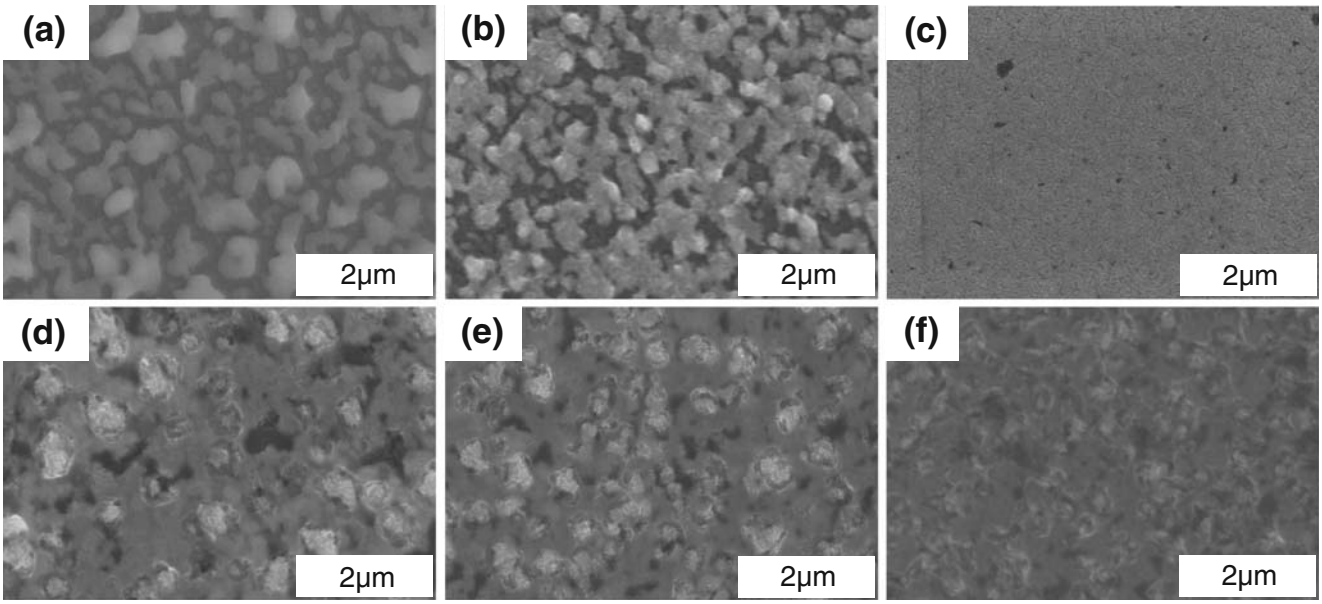

Fig. 3 SEM images of (**a**) 5 m/o Zr–Cu, (**b**) 7.5 m/o Zr–Cu, (**c**) 10 m/o Zr–Cu, (**d**) 15 m/o Zr–Cu, (**e**) 20 m/o Zr–Cu, and (**f**) 30 m/o Zr–Cu film annealed at 900°C in a reducing ambient

described here suggest that solution-based processing may be attractive for some applications.

Figure 5 shows the thickness dependence of the electrical resistivity of 10 m/o Zr–Cu films. It was found that films ≤60 nm thick could not be measured after annealing at 900°C because of the discontinuous microstructure. For thicker films, the resistivity of 10 m/o Zr–Cu films decreases with increasing film thickness and approximately saturates for layer thicknesses of 100 nm. It is well known that the resistivity of thin films increases with decreasing film thickness due to the scattering of conduction electrons at the free surfaces and interfaces [34, 39]. In addition, the influence of grain boundary scattering on resistivity should be considered in polycrystalline thin films [40]. It is possible that the difference between the lowest resistivity of the CSD copper films produced here and the bulk resistivity of copper results from a combination of the small film grain size, and additional impurity scattering due to the adhesion promoter.

Figure 6 shows the effect of the oxygen partial pressure during firing on the electrical resistivity of Zr-doped Cu films. It is not surprising that as the oxygen partial pressure increases, the resistivity of the films also increases. Films annealed at $PO_2 \sim 10^{-12}$ atm have peaks of ZrO_2 and Cu_2O

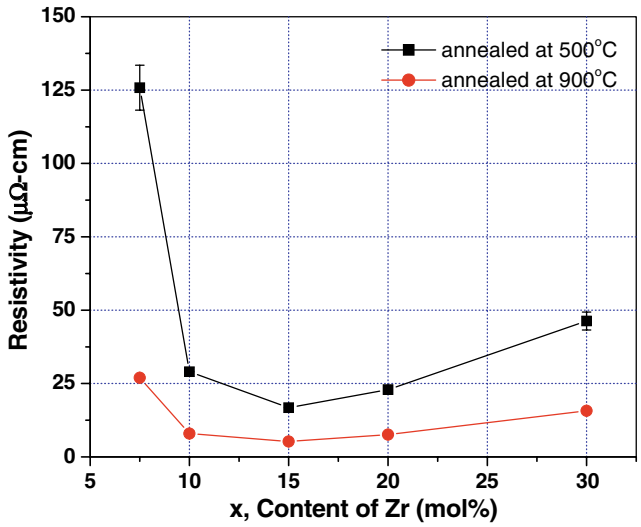

Fig. 4 The resistivity of 80 nm thick Zr-doped Cu film with different compositions

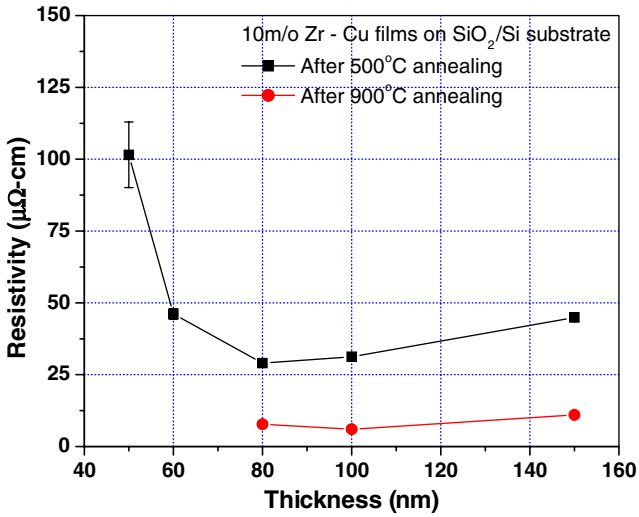

Fig. 5 The resistivity of 10 m/o Zr–Cu film with different thicknesses prepared at different processing temperatures

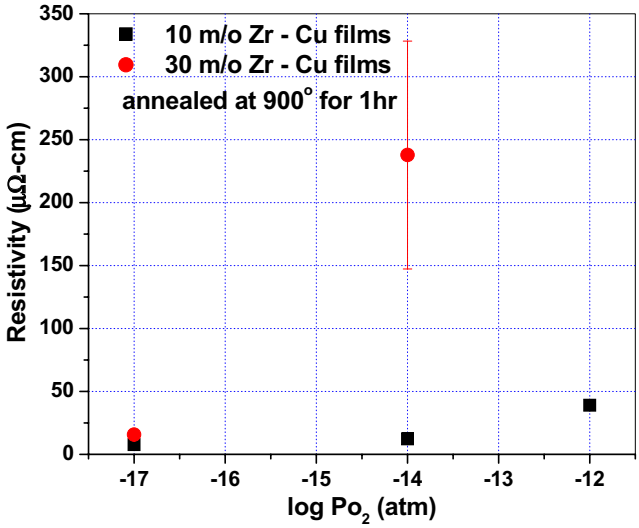

Fig. 6 The resistivity of Zr-doped Cu film processed at different oxygen partial pressures

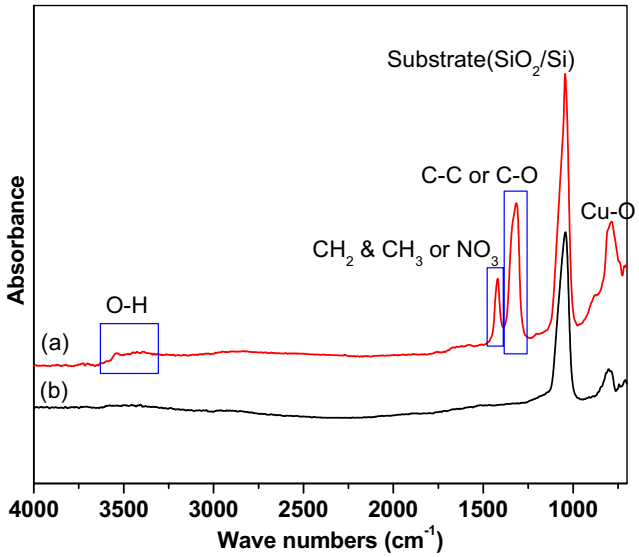

Fig. 8 FT-IR-ATR data of 10 m/o Zr–Cu film (**a**) after 130°C pyrolysis and (**b**) after 290°C annealing in a reducing ambient

irrespective of Zr content as seen in Fig. 7. The crystallinity of the Cu also decreases with increasing oxygen partial pressure. All of the films with 30 m/o Zr–Cu annealed at 900°C showed ZrO_2 peaks (not shown here). The existence of ZrO_2 and Cu_2O contributes to the increased resistivity of Cu films with high Zr contents.

Elemental copper should be stable at $PO_2 \sim 10^{-12}$ atm at 900°C according to the Ellingham diagram [41], but the measured XRD patterns show the existence of copper oxide. There are several possible reasons for this. First, if the film retains carbon or nitrogen after pyrolysis, removal of these species at high temperatures can locally change the oxygen partial pressures. To assess this possibility, CSD-derived Cu powder was prepared by heating a Zr-doped Cu solution at 150°C for 24 h to remove the liquid organics. It was found using thermal gravimetric analysis that complete decomposition occurs around 225°C with air and 350°C with nitrogen. The pyrolysis temperature used for the Cu film was over 250°C in an air ambient, so the films should not have significant organic residue. In order to confirm this, Cu films pyrolyzed at different temperatures were analyzed by FT-IR-ATR (Fourier Transform Infrared Attenuated Total Reflectance). In Fig. 8(a), a broad absorption band corresponding to the OH stretch was observed near 3,400 cm^{-1} after the 130°C heat treatment in air. In addition, peaks corresponding to the CH_2 group,

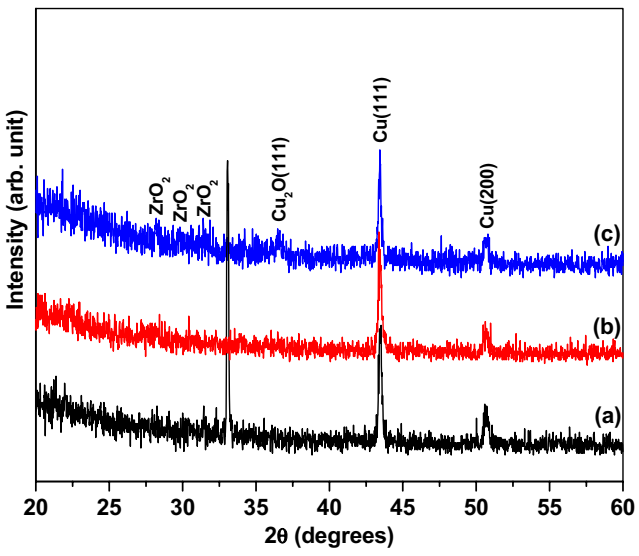

Fig. 7 XRD patterns of 10 m/o Zr–Cu film annealed at 900°C at different oxygen partial pressures: (**a**) 10^{-17} atm, (**b**) 10^{-14} atm and (**c**) 10^{-12} atm

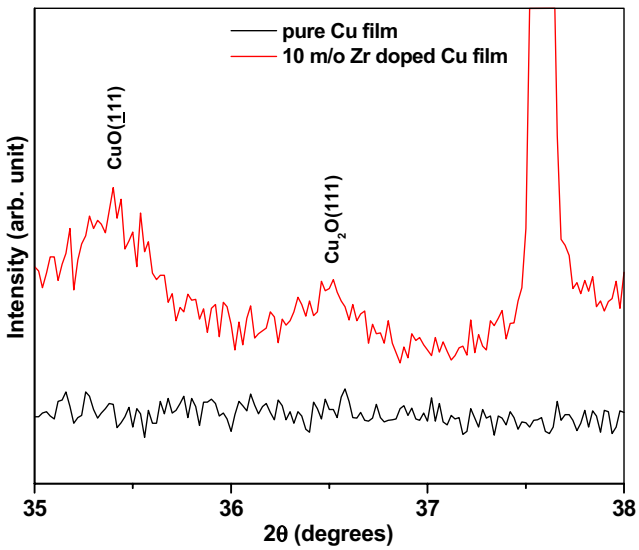

Fig. 9 XRD patterns of pure Cu film and 10 m/o Zr–Cu film annealed at 900°C at oxygen partial pressures ~10^{-14} atm

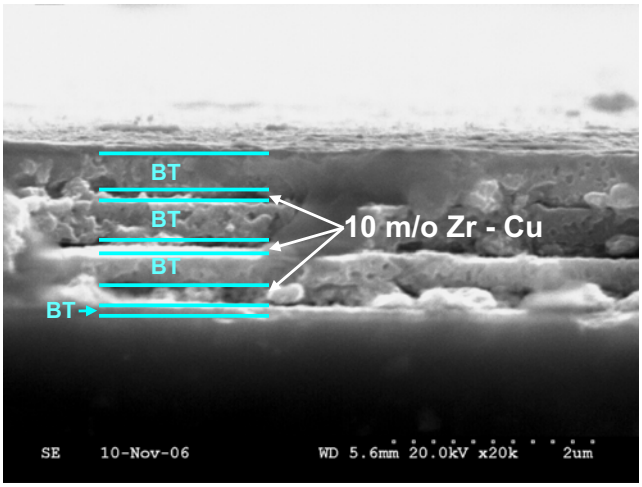

Fig. 10 SEM image of cross-section of multilayer capacitor using $BaTiO_3$ and 10 m/o Zr–Cu solutions

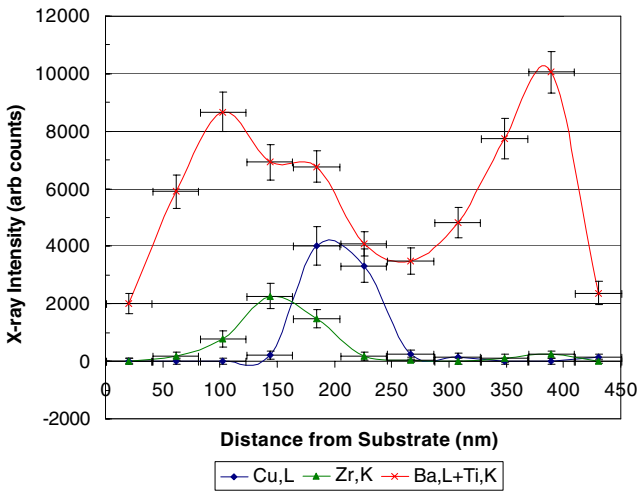

Fig. 12 TEM-EDS profiles of $BaTiO_3$/Cu/$BaTiO_3$ capacitor on sapphire substrate

the CH_3 group, the NO_3 group, the C–O and the C–C single bond were observed around 1,420 and 1,315 cm^{-1} respectively [42, 43]. However, there is no organic residue after a 290°C heat treatment in air as seen in Fig. 8(b). This result is consistent with the thermal gravimetric analysis. Therefore, retained carbon is not the main cause of Cu oxide formation.

A second possibility is that the film may be exposed to a high oxygen partial pressure during heating and cooling as described by Kingon et al. [44]. Figure 9 shows XRD patterns for a pure Cu film and a 10 m/o Zr-doped Cu film annealed at 900°C for 1 h at 10^{-14} atm PO_2. A long scan (5 s per step) was used to increase the sensitivity to the presence of Cu_2O. As seen in Fig. 9, exposure to an excessively high oxygen partial pressure during heating and cooling is probably not dominant in this work, since pure Cu films can be made even though copper oxide is formed after pyrolysis. Therefore, it seems that the Zr content is related to the formation of copper oxide. The solid solubility of Zr in Cu is less than 0.12 at% [45] and Zr may diffuse to the surfaces of the film after 700°C annealing [34]. Therefore, at least some of the Zr may exist near the interfaces as an oxide (ZrO_2 is stable at the oxygen partial pressure used based on the Ellingham diagram). This ZrO_2 layer might retard movement of oxygen out of the Cu layer.

In order to check the compatibility between CSD Zr doped Cu films and $BaTiO_3$, a, multilayer Cu/$BaTiO_3$ stack was fabricated. $BaTiO_3$, Cu and $BaTiO_3$ layers were spin-coated onto the substrate in sequence. The sample was pyrolyzed at 350°C for 3 min after each deposition. After

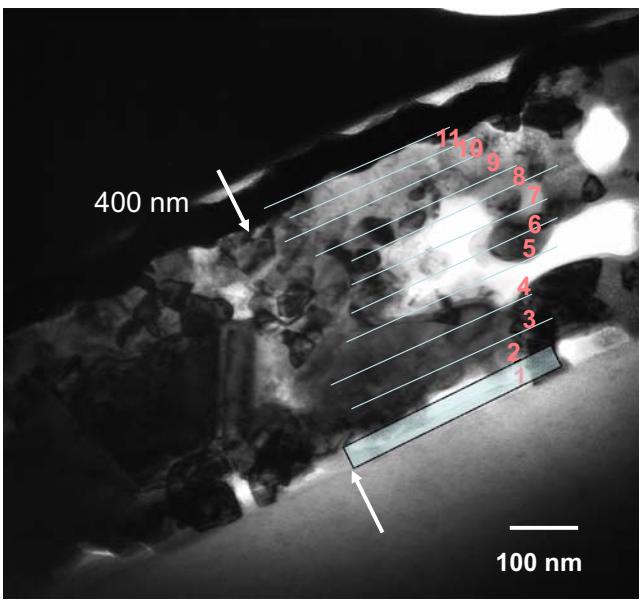

Fig. 11 TEM image of cross-section of $BaTiO_3$/Cu/$BaTiO_3$ capacitor on sapphire substrate by chemical solution deposition

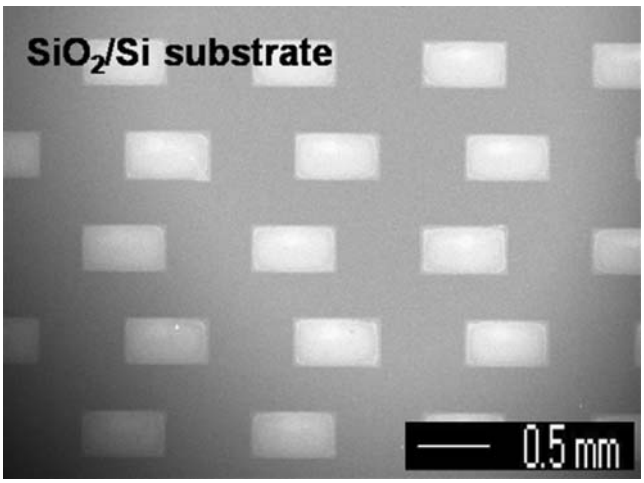

Fig. 13 Optical image of patterns of microcontact printed 10 m/o Zr doped Cu

all depositions, the multilayer sample was annealed in tube furnace in a reducing ambient. An Al_2O_3 single crystal (MTI corporation, Richmond, CA) was used as a substrate because its coefficient of thermal expansion is closer to that of $BaTiO_3$ than is that of a Si substrate. The deposition conditions are comparable to those reported by Nagata for the $BaTiO_3$ [7], and those described here for the Cu. The multilayer capacitor was annealed using three different annealing steps, as proposed by Hakotani et al. [46]. They reported forming multilayer laminates by a green tape process using dielectric ceramic tapes and a conductor paste containing CuO as its main component. The three annealing steps used were: binder removal (600°C in air), reduction (400°C in N_2+H_2) and sintering (950°C in N_2). However, we found that the Cu film peeled off when Zr contents ≤3 m/o were used, while Cu films with ≥5 m/o Zr did not peel off after first step. These data confirm the role of ZrO_2 as an adhesion promoter for $BaTiO_3$, as was the case for SiO_2 surfaces. It was also found that multilayer samples were cracked after the final step. This might be from the volume change on conversion of CuO to Cu. To avoid this, a modified annealing scheme was employed: crystallization (900°C in N_2), reduction (450°C in N_2+H_2) and re-oxidation (550°C in N_2). Only Cu_2O and $BaTiO_3$ were detected after the first step. Figure 10 shows a cross-sectional SEM image of the multilayer. It is clear that CSD capacitor multilayers can be prepared using base metal electrodes and that there is no evidence of cracking or delamination. Figure 11 shows a TEM image of a $BaTiO_3$/Cu/$BaTiO_3$/sapphire capacitor and Fig. 12 a compositional depth profiles of the sample. For the composition analysis, the film structure was sampled via EDS in 40 nm slices. Some of slices include voids as seen in Fig. 11. Theses voids are believed to be the origin of big dip in intensity of Ba and Ti between 200 nm and 350 nm depth. Of particular interest from the standpoint of integrated capacitor applications is the observation that ZrO_2 was observed to segregate to the surfaces of the Cu layer based on the EDS depth profiles.

The microcontact printability of copper solution is also important for several applications. To assess this, polydimethylsiloxane (PDMS) was used as a stamp; the procedure for making the stamp had been described elsewhere [7]. The copper precursor solution was deposited onto a dried PDMS stamp and spin cast at 3,000 rpm for 30 s. The stamp then was brought into contact with a SiO_2/Si substrate surface to transfer the copper precursor. Figure 13 shows an optical image of the transferred copper patterns. The height of the pattern is about 60 nm after a 260°C pyrolysis. It is clear that the copper precursor solution can be transferred to oxide substrates without degradation of the features.

4 Conclusions

This paper demonstrates preparation of copper films by chemical solution deposition. These copper films show good electrical properties (the resistivities of 80 nm thick 15 m/o Zr–Cu film are 16–17 μΩ-cm after 500°C annealing and 5–6 μΩ-cm after 900°C annealing). The films can be patterned by micro-contact printing without requiring photolithography. Also, dewetting of copper from oxide surfaces can be avoided using adhesion promoters/film stabilizers like Ti, Zn, and Zr and the appropriate profile for the heat treatment.

Acknowledgments This work was supported by KEMET Electronics Corporation.

References

1. H. Kishi, Y. Mizuno, H. Chazono, Base–metal electrode-multilayer ceramic capacitors: past, present and future perspectives Jpn. J. Appl. Phys. **42**(1), 1–15 (2003), Part 1
2. C.A. Randall, Scientific and Engineering issues of the state-of-the-art and future multilayer capacitors J. Ceram. Soc. Jpn. **109**(1), S2–S6 (2001)
3. M. Randall, D. Skamser, T. Kinard, J. Qazi, A. Tajuddin, S. Trolier-McKinstry, C. A. Randall, S. W. Ko, T. Dechakupt, Thin Film MLCC, *CARTS* 2007 (2007)
4. J.W. Crownover, US Patent No. 5,254,360 (1993)
5. Y. Sakabe, Development of dielectric ceramics for nickel electrode multilayer capacitors J. Jpn. Soc. Powder Powder Metallurgy **51** (4), 274–284 (2004)
6. J.T. Dawley, P.G. Clem, Dielectric Properties of random and <100> oriented $SrTiO_3$ and (Ba,Sr)TiO_3 thin films fabricated on <100> nickel tapes Appl. Phys. Lett. **81**(16), 3028–3030 (2002). doi:10.1063/1.1516630
7. H. Nagata, S.W. Ko, E. Hong, C.A. Randall, S. Trolier-McKinstry, P. Pinceloup et al., Microcontact printed $BaTiO_3$ and $LaNiO_3$ thin films for capacitors J. Am. Ceram. Soc. **89**(9), 2816–2821 (2006)
8. T. Dechakupt, G. Yang, C.A. Randall, I. Reaney, S. Trolier-McKinstry, Chemical solution-deposited $BaTiO_3$ thin films on Ni foils: microstructure and interfaces J. Am. Ceram. Soc. **91**(6), 1845–1850 (2008). doi:10.1111/j.1551-2916.2008.02407.x
9. J. Ihlefeld, B. Laughlin, A. Hunt-Lowery, W. Borland, A. Kingon, J.-P. Maria, Copper compatible barium titanate thin films for embedded passives J. Electroceram. **14**, 95–102 (2005). doi:10.1007/s10832-005-0866-6
10. J. Ihlefeld, W. Borland, J.-P. Maria, Enhanced dielectric and crystalline properties in ferroelectric barium titanate thin films Adv. Funct. Mater. **17**, 1199–1203 (2007). doi:10.1002/adfm.200601159
11. W. Borland, J. Ihlefeld, A.I. Kingon, J.-P. Maria, Thin film dielectric for capacitors and methods of making thereof. U.S. Patent 7,029,971, April 18, 2006
12. Y. Sakabe, Y. Takeshima, K. Tanaka, Multilayer ceramic capacitors with thin (Ba,Sr)TiO_3 Layers by MOCVD J. Electroceram. **3**(2), 115–121 (1999). doi:10.1023/A:1009986825169
13. Y. Yamashita, H. Yamamoto, Y. Sakabe, Dielectric properties of $BaTiO_3$ thin films derived from clear emulsion of well-dispersed

nanosized $BaTiO_3$ particles Jpn. J. Appl. Phys. **43**(9B), 6521–6524 (2004). doi:10.1143/JJAP.43.6521
14. M.M. Watt, P. Woo, T. Rywak, L. McNeil, A. Kassam, V. Joshi, et al., Feasibility demonstration of a multi-level thin film BST capacitor technology. ISAF 98, Proceedings of the Eleventh IEEE International Symposium 11–14 (1998)
15. G.L. Brennecka, B.A. Tuttle, Fabrication of ultrathin film capacitors fabricated by chemical solution deposition J. Mater. Res. **22**(10), 2868–2874 (2007). doi:10.1557/jmr.2007.0371
16. G.L. Brennecka, C.M. Parish, B.A. Tuttle, L.N. Brewer, Multi-layer thin and ultrathin film capacitors fabricated by chemical solution deposition J. Mater. Res. **23**(1), 176–181 (2008). doi:10.1557/jmr.2008.0010
17. S. Miyake, K. Yamamoto, S. Fujihara, T. Kimura, (100)-orientation of pseudocubic perovskite-type $LaNiO_3$ thin films on glass substrates via the sol–gel process J. Am. Ceram. Soc. **85**, 992–994 (2002)
18. J. Li, J.W. Mayer, E.G. Colgan, Oxidation and protection in copper and copper alloy thin films J. Appl. Phys. **70**(5), 2820–2827 (2002). doi:10.1063/1.349344
19. H.K. Liou, J.S. Huang, K.N. Tu, Oxidation of Cu and Cu_3Ge thin films J. Appl. Phys. **77**(10), 5443–5445 (1995). doi:10.1063/1.359238
20. P. Shen, H. Fujii, K. Nogi, Wetting, adhesion and diffusion in Cu–Al/SiO_2 system at 1473K Scr. Mater. **52**, 1259–1263 (2005). doi:10.1016/j.scriptamat.2005.02.019
21. M. Hu, S. Noda, T. Okubo, H. Komiyama, Wettability and crystalline orientation of Cu nanoislands on SiO_2 with a Cr underlayer Appl. Phys. A **79**, 625–628 (2004). doi:10.1007/s00339-004-2604-3
22. S.-F. Wang, T.C.K. Yang, S.-C. Lee, Wettability of Electrode Metals on Barium Titanate Substrate J. Mater. Sci. **36**, 825–829 (2001). doi:10.1023/A:1004862011318
23. D.P. Cann, J.-P. Maria, C.A. Randall, Relationship between wetting and electrical contact properties of pure metals and alloys on semiconducting barium titanate ceramics J. Mater. Sci. **36**, 4969–4976 (2001). doi:10.1023/A:1011817128242
24. R. Standing, M. Nicholas, The wetting of alumina and vitreous carbon by copper–tin–titanium alloys J. Mater. Sci. **13**, 1509–1514 (1978). doi:10.1007/BF00553207
25. A. Kar, S. Mandal, S. Rathod, A.K. Ray, Effect of Ti diffusivity on the formation of phases in the interface of alumina–alumina brazed with $97(Ag_{40}Cu)_3Ti$ filler alloy. *Proceedings the 3*rd *international brazing and soldering conference*. April 24–26 San Antonio, Texas, USA (2006).
26. M. Hu, S. Noda, T. Okubo, H. Komiyama, Wettability and crystalline orientation of Cu nanoislands on SiO_2 with a Cr Underlayer Appl. Phys. A **79**, 625–628 (2004). doi:10.1007/s00339-004-2604-3
27. M. Hu, S. Noda, T. Okubo, Y. Yamaguchi, H. Komiyama, Structural and morphological control of nanosized Cu islands on SiO_2 using a Ti underlayer J. Appl. Phys. **94**(5), 3492–3497 (2003). doi:10.1063/1.1597972
28. P.B. Abel, A.L. Korenyi-Both, F.S. Honecy, S.V. Pepper, Study of copper on graphite with titanium or chromium bond layer J. Mater. Res. **9**(3), 617 (1994). doi:10.1557/JMR.1994.0617
29. O.-K. Kwon, S.-H. Kwon, H.-S. Park, S.-W. Kang, PEALD of a ruthenium adhesion layer for copper interconnects J. Electrochem. Soc. **151**(12), C753–C756 (2004). doi:10.1149/1.1809576
30. Z. Wang, O. Yaegashi, H. Sakaue, T. Takayuki, S. Shingubara, Highly adhesive electroless Cu layer formation using an ultra thin Ionized Cluster Beam (ICB)-Pd catalytic layer for sub-100nm Cu interconnections Jpn. J. Appl. Phys. **42**, L1223–L1225 (2003). doi:10.1143/JJAP.42.L1223
31. F. Alvarez y Quintavalle, G.A. Battiston, U. Casellato, D. Fregona, R. Gerbasi, F. Loro, Conductive Cu-TiO_2 thin films obtained via MOCVD J. Phys. IV Fr. **12**, Pr4–Pr147 (2002)
32. N. Awaya, Y. Arita, Plasma-enhanced chemical vapor deposition of copper Jpn. J. Appl. Phys. **30**, 1813–1817 (1991). doi:10.1143/JJAP.30.1813
33. J.Y. Kim, P.J. Reucroft, D.K. Park, Nucleation and growth of mechanisms of copper MOCVD film on Au/Si substrates Thin Solid Films **289**, 184–191 (1996). doi:10.1016/S0040-6090(96)08908-0
34. C.J. Liu, J.S. Chen, Influence of Zr additives on the microstructure and oxidation resistance of Cu(Zr) thin films J. Mater. Res. **20**(2), 496–503 (2005). doi:10.1557/JMR.2005.0068
35. J.-W. Lim, K. Mimura, M. Isshiki, Thickness dependence of resistivity for Cu films deposited by ion beam deposition Appl. Surf. Sci. **217**, 95–99 (2003). doi:10.1016/S0169-4332(03)00522-1
36. D.P. Cann, C.A. Randall, Segregation in bimetallic alloys and its influence on wetting on a positive temperature coefficient resistor $BaTiO_3$ ceramic J. Appl. Phys. **90**(11), 5698–5702 (2001). doi:10.1063/1.1413237
37. D.P. Cann, C.A. Randall, The thermochemistry and non-ohmic electrical contacts of a $BaTiO_3$ PTCR Ceramic IEEE Trans. Ultrason. Ferroelectr. Freq. Control **44**(6), 1405–1408 (1997). doi:10.1109/58.656645
38. K. Lee, Y.K. Lee, Irreversible hydrogen effects on resistivity of sputtered copper film J. Mater. Sci. **35**, 6035–6040 (2000). doi:10.1023/A:1026727818193
39. A.F. Mayadas, R. Feder, R. Rosenberg, Resistivity and structure of evaporated aluminum films J. Vac. Sci. Technol. **6**, 690–693 (1969). doi:10.1116/1.1315731
40. A.F. Mayadas, M. Shatzkes, Electrical-resistivity model for polycrystalline films: the case of arbitrary reflection at external surfaces Phys. Rev. B **1**, 1382–1389 (1970). doi:10.1103/PhysRevB.1.1382
41. T.-H. Song, C.A. Randall, Copper cofire X7R dielectrics and multilayer capacitors based on zinc borate fluxed barium titanate ceramic J. Electroceram. **10**, 39–46 (2003). doi:10.1023/A:1024028024779
42. J. Coates, *Encyclopedia of Analytical Chemistry* (Wiley, New York, 2000)
43. J.R. Martinez, G. Ortega-Zarzosa, O. Dominguez-Espinos, F. Ruiz, Low temperature devitrification of Ag/SiO_2 and Ag(CuO)/SiO_2 composites J. Non-cryst Solids **282**, 317–320 (2001). doi:10.1016/S0022-3093(01)00346-5
44. A.I. Kingon, S. Srinivasan, Lead zirconate titanate thin films directly on copper electrodes for ferroelectric, dielectric and piezoelectric applications Nat. Mater. **4**, 233–237 (2005). doi:10.1038/nmat1334
45. T.B. Massalski, *Binary Alloy Phase Diagrams*, 2nd edn. (ASM, Materials Park, OH, 1990)
46. Y. Hakotani, US Patent No., 5,004,715 (1991)